Ultraviolet Photodissociation Dynamics of the Propargyl Radical†

Xianfeng Zheng,‡ Yu Song, and Jingsong Zhang*

Department of Chemistry, University of California at Riverside, Riverside, California 92521

Received: December 22, 2008

Ultraviolet (UV) photodissociation dynamics of jet-cooled propargyl (C_3H_3) radical is studied in the photolysis wavelength region of 230 to 250 nm with high-*n* Rydberg atom time-of-flight (HRTOF) and resonance enhanced multiphoton ionization (REMPI) techniques. In this wavelength region, the photofragment yield (PFY) spectra of the H + C_3H_2 product channel are obtained by using propargyl chloride, allene, and propyne as precursors of the C_3H_3 radicals, and they have a broad peak centered near 240 nm and are in good agreement with the previous UV absorption spectrum of C_3H_3 by Fahr et al. The H + C_3H_2 product translational energy distributions, $P(E_T)$'s, are obtained from all three precursors and are essentially the same. The $P(E_T)$ distributions peak at ~5 kcal/mol, and the fraction of average translational energy in the total excess energy, $\langle f_T \rangle$, is ~0.3. The H-atom product angular distribution is isotropic, with the anisotropy parameter $\beta \approx 0$. The dissociation mechanism is consistent with internal conversion of the electronically excited propargyl followed by unimolecular decomposition on the ground state. Our study supports the previously observed UV absorption spectrum of propargyl near 240 nm by Fahr et al. and is in general agreement with the results in the UV photodissociation of propargyl by the groups of Chen and Neumark, but disagrees with the recent theoretical calculations by Eisfeld.

Introduction

Propargyl radical ($HCCCH_2$) is a prototypical conjugated hydrocarbon radical, and it is also an important intermediate in hydrocarbon combustion, particularly in its recombination reaction to form the first aromatic ring and in the subsequent production of polycyclic aromatic hydrocarbons (PAH) and soot.[1−4] Consequently, the electronic states and spectroscopy of the C_3H_3 radical have been studied extensively by both theories and experiments.

The propargyl radical was first identified by Farmer and Lossing in a mass spectrometric study that determined its ionization potential.[5] The first electronic absorption spectrum of the C_3H_3 radical was recorded by Ramsay and Thistlethwaite in the photolysis of propargyl bromide, propargyl chloride, methyl acetylene, allene, and other compounds.[6] A series of diffuse bands were found between 290 and 345 nm, and the diffuseness of the bands was attributed to predissociation in the excited state and gave an upper limit of 86.0 kcal/mol for the bond dissociation energy (BDE) of the propargyl radical. This near-ultraviolet (UV) absorption spectrum was later confirmed in the region between 280 and 370 nm by matrix isolation spectroscopy[7,8] and cavity ringdown spectroscopy[9] by using various precursors. This near-UV absorption band was assigned to the dipole-allowed $2^2B_1 \leftarrow \tilde{X}^2B_1$ transition.[8,10]

The second absorption band of the propargyl radical was first reported in the UV range of 230−300 nm by Fahr et al.[11] The UV absorption spectra of the propargyl radicals produced from the C_3H_3Cl and C_3H_3Br precursors by both photolysis and abstraction reaction were nearly identical. The UV absorption band had a broad peak with a maximum at 242 nm and was much stronger than the first absorption band in the near-UV region. The UV band was assigned to the dipole-allowed $3^2B_1 \leftarrow \tilde{X}^2B_1$ transition.[10,11] This UV absorption spectrum was confirmed by H-atom product action spectrum in the UV photodissociation of the propargyl radical by Deyerl et al.[12] However, this strong UV absorption band of propargyl was questioned, as it was not observed in a later study with halogen-free precursors,[13] and thus was attributed to chlorine and bromine adducts of propargyl halides (such as $C_3H_3Cl_2$).[9,14] Fahr and Laufer then rechecked the UV absorption spectra between 220 and 350 nm of transient species generated from 193-nm photolysis of allene, propyne, and 2-butyne.[15] A strong band around 240 nm and a weaker band in the 330 nm region were identified, similar to their early results with the C_3H_3Cl and C_3H_3Br precursors.[11] This recent study indicated that the strong UV absorption feature peaking at 242 nm may not be due to the halogenated adducts and the spectrum with the allene precursor was most likely from the propargyl radical.[15]

The electronic states of the propargyl radical have also been examined by theoretical studies.[10,11,16−19] The propargyl radical, $HCCCH_2$, was shown to be the lowest energy structure of C_3H_3, and the molecular geometry and electronic structure of the $\tilde{X}^2B_1$ ground state of propargyl were examined.[16,17] The lowest two doublet excited states were identified by Honjou et al. to be 1^2B_2 and 2^2B_1 in C_{2v} symmetry, and they relax to lower energy states $1^2A''$ and $2^2A'$ in C_s symmetry, respectively.[16,19] The transition from the $\tilde{X}^2B_1$ ground state to the lowest excited state 1^2B_2 is dipole forbidden, while the near-UV absorption band in the region of 280 to 370 nm was assigned to the dipole-allowed $2^2B_1 \leftarrow \tilde{X}^2B_1$ transition.[10] The next higher excited states are 2^2B_2 and 3^2B_1.[10,11,16,17] Fahr et al. assigned the strong absorption feature peaking at 242 nm to the dipole-allowed $3^2B_1 \leftarrow \tilde{X}^2B_1$ transition based on their calculated vertical excitation energy.[11] However, Eisfeld recently calculated the four electronically excited states 1^2B_2, 2^2B_1, 2^2B_2, and 3^2B_1 and the absorption spectrum of C_3H_3 in the region from 180 to 400 nm.[10,17] While

† Part of the "George C. Schatz Festschrift".

* Corresponding author. E-mail: jingsong.zhang@ucr.edu. This author is also at Air Pollution Research Center, University of California, Riverside, CA 92521.

‡ Permanent address: Department of Physics, Anhui Normal University, Wuhu, Anhui 241000, People's Republic of China.

10.1021/jp8113336 CCC: $40.75
Published on Web 03/10/2009

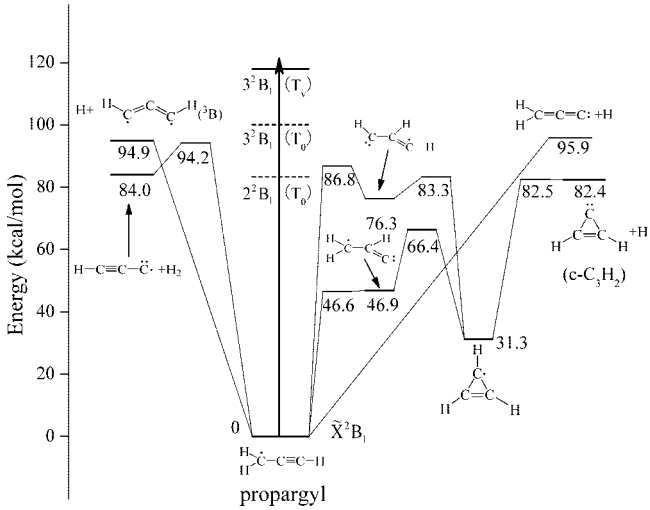

Figure 1. Potential energy diagram of the C_3H_3 system. The three H-atom dissociation pathways and the H_2 elimiantion pathway are shown in the figure. The energetics and pathways are based on the theoretical calculations in ref 19. The energies of the C_3H_3 excited states are based on refs 8, 10, 11, 16, and 17. The adiabatic energy T_0 of 2^2B_1 is from Wyss et al.,[8] and T_0 and vertical energy T_v of 3^2B_1 are estimated from the absorption spectrum by Fahr et al.[11]

the dipole-allowed $2^2B_1 \leftarrow \tilde{X}^2B_1$ band agreed well with the near-UV absorption spectrum, the dipole-allowed $3^2B_1 \leftarrow \tilde{X}^2B_1$ transition was predicted to be a much weaker band with the vertical energy near 220 nm and the dipole-forbidden $2^2B_2 \leftarrow \tilde{X}^2B_1$ transition was also very weak and peaked near 260 nm.[10,17] It was then concluded that the strong UV absorption observed near 242 nm by Fahr et al.,[11] as well as the H-atom product signals and the H-atom action spectrum observed by Deyerl et al.,[12] was not due to the propargyl radical but some other transient species.[10]

Photodissociation of the propargyl radical has been investigated by both theory and experiments.[12,20−23] The potential energy diagram of the ground electronic state[18−20] and the dissociation pathways for the H atom and H_2 elimination channels of C_3H_3 are shown in Figure 1. There are three H atom loss channels to different C_3H_2 isomers that are close in energy and one H_2 loss channel,

$$H_2CCCH(\tilde{X}^2B_1) + h\nu \rightarrow c\text{-}C_3H_2(^1A_1) + H, \quad \Delta H_{rxn,0} = 82.4 \text{ kcal/mol}$$

$$\rightarrow HCCCH(^3B) + H, \quad \Delta H_{rxn,0} = 94.9 \text{ kcal/mol}$$

$$\rightarrow H_2CCC(^1A_1) + H, \quad \Delta H_{rxn,0} = 95.9 \text{ kcal/mol}$$

$$\rightarrow HCCC(^2A') + H_2, \quad \Delta H_{rxn,0} = 84.0 \text{ kcal/mol}$$

The energetics are based on the recent high-level theoretical calculations by Nguyen et al.,[19,20] which are in reasonable agreement with the thermochemistry data.[19,20,24] The UV photodissociation of propargyl was first studied in the secondary photolysis of hot propargyl radical produced in 193 nm photodissociation of allene.[21] Both the C_3H_2 + H and C_3H + H_2 product channels were identified, with a branching ratio of 0.94 to 0.04. The photofragment translational energy distribution $P(E_T)$ showed that the product translational energy release of the C_3H_2 + H channel was modest, peaking at ~12.5 kcal/mol and with the fraction of average kinetic energy in the total excess energy, $\langle f_T \rangle$, being ~0.31. The UV photodissociation dynamics of jet-cooled propargyl radical produced from flash pyrolysis of propargyl bromide was examined in the region of 240 to 265 nm by Chen's group.[12] The H atom product from the C_3H_2 + H channel was ionized by 1 + 1′ (Lyman-α + 365 nm radiation) resonance enhanced multiphoton ionization (REMPI) and then detected by a time-of-flight mass spectrometer (TOFMS). The H-atom Doppler profile was measured to provide the $P(E_T)$ distribution that peaked at ~2.5 kcal/mol and with $\langle E_T \rangle \approx 6.2$ kcal/mol and $\langle f_T \rangle \approx 0.22$. The shape of the $P(E_T)$ distribution is close to that in a prior distribution,[12] and indicated a mechanism in which the electronically excited propargyl decayed via internal conversion to the ground state followed by unimolecular decomposition. A statistical analysis of the energetics suggested that the dominant channel in the photodissociation of propargyl radical at 242 nm was the formation of cyclopropenylidene, c-C_3H_2 + H. By using partially deuterated propargyl radical, H_2CCCD, nearly complete isotopic scrambling was observed, and the dissociation mechanism was shown to proceed via an initial 1,2 H-shift followed by cyclization.

Nguyen et al. investigated theoretically the photodissociation of propargy radical at photon energies of 193 and 242 nm, assuming that the electronically excited propargyl radical underwent internal conversion to the ground electronic state followed by unimolecular decomposition.[19,20] RRKM rate constant calculations for the various dissociation channels were carried out on the potential energy surface obtained with high-level theory.[19,20] The calculated product branching ratios for the C_3H_2 + H and C_3H + H_2 channels at 193 nm were in good agreement with the experimental measurements in the secondary photolysis of C_3H_3.[21] The product branching ratios at 242 nm were calculated to be 90.2% for $HCCCH(^3B)$ + H, 5.1% for c-$C_3H_2(^1A_1)$ + H, 1.6% for $H_2CCC(^1A_1)$ + H, 3.0% for $HCCC(^2A')$ + H_2, and 0.1% for $CH(^2\Pi)$ + C_2H_2. The $HCCCH(^3B)$ + H were predicted to be the major products while the c-C_3H_2 + H channel, although energetically the most favorable H loss channel, was calculated to be minor. These results were in disagreement with those from the experimental study by Chen's group,[12] where c-C_3H_2 + H was shown to be the major product.

Most recently, Neumark's group investigated the photodissociation of the jet-cooled propargyl radical and its perdeuterated isotopologue using photofragment translational spectroscopy.[23] The propargyl radicals were produced from 193 nm photolysis of allene, and photodissociated at 248 nm. Both the H loss and H_2 loss dissociation channels were characterized by observations of the counterparts C_3H_2 and C_3H, respectively. The branching ratio for H loss/H_2 loss was 97.6/2.4 ± 1.2, in agreement with the value of 96.9/3.0 from the RRKM calculations by Nguyen et al.[20] The average translational energy, $\langle E_T \rangle$, for the H loss and H_2 loss channels was 5.7 and 15.3 kcal/mol, respectively. The $P(E_T)$ distribution for the H atom loss was similar to that by Chen's group and the prior distribution[12] and peaked at 1.8 kcal/mol. The $P(E_T)$ distributions of the photofragments indicated that internal conversion to the ground electronic state occurred following the excitation to the excited electronic state, and that the ground state propargyl dissociated to H + C_3H_2 via a loose transition state without an exit channel barrier while to H_2 + C_3H via a tight transition state with an exit barrier.[23] The decomposition of hot ground state propargyl was also studied in the secondary dissociation of the propargyl radical produced in 157 nm photodissociation of the propargyl chloride.[22] Both the H loss and H_2 loss were observed via the secondary fragments of propargyl. On the basis of the difference between the translational energy distributions of the Cl atom

and the propargyl radical fragments, a propargyl dissociation energy (or barrier) of 71.5 (+5/−10) kcal/mol was suggested,[22] which is more than 10 kcal/mol lower than the theoretical and thermochemistry values.[19]

This current work investigates the UV photodissociation dynamics of the jet-cooled propargyl radical in the photolysis wavelength region of 230−250 nm by using three different precursors, propargyl chloride, allene, and propyne. This study aims to probe the photodissociation dynamics of C_3H_3 via the 3^2B_1 excited state, confirm the origin of the previously observed broad absorption peak of propargyl near 240 nm and the H-atom photodissociation,[11,12] and search for the possible absorption bands of propargyl that were predicted by the theory.[10] Propargyl chloride, allene, and propyne provide both halogen and halogen-free precursors of propargyl, and moreover they have less absorption at 230−250 nm (thus less interference to the propargyl radical photodissociation) than the propargyl bromide precursor.[11,12] The H-atom photofragment yield (PFY) spectra of propargyl radicals produced from the three precursors are measured with the REMPI technique, and are compared with the UV absorption spectrum of C_3H_3 near 240 nm to confirm this broad absorption of propargyl. The product translational energy and angular distributions for the H + C_3H_2 channel are obtained by detecting the H-atom products with the high-*n* Rydberg atom time-of-flight (HRTOF) technique. Our approach is complementary to the previous studies by the groups of Chen and Neumark;[12,23] the HRTOF technique has a higher resolution than the H-atom Doppler profile, and HRTOF also has less interference for the low kinetic energy products compared to the H-atom Doppler profile and the TOF spectra of the heavy fragment C_3H_2 (which recoiled little from the parent C_3H_3 beam). By directly providing reliable $P(E_T)$ and angular distributions with use of the three different precursors, the photodissociation signals and dynamics of the propargyl radical are further established. To compare with recent theory,[10] REMPI detection of C_3H_3, in addition to the H-atom PFY spectra, is also attempted in the region of 220−280 nm.

Experimental Section

The HRTOF technique and experimental setup have been described previously.[25−27] A pulsed C_3H_3 radical beam was generated by photolyzing propargyl chloride (purity ≥98%), allene (purity ≥99.7%), or propyne (purity ≥99.7%) precursors seeded in Ar or He (at ∼4% concentration and a total pressure of 120 kPa),[9,11,15] with the 193-nm radiation of an ArF excimer laser that was focused in front of the pulse nozzle. The C_3H_3 radicals produced from the photolysis were entrained in the seeded beam and subsequently cooled by supersonic expansion. The radical beam was collimated at 2.8 cm downstream by a 1-mm-diameter skimmer into a high-vacuum chamber; at 4.6 cm further downstream of the skimmer, the C_3H_3 radical beam was crossed with a slightly focused UV photolysis laser radiation (at 230−250 nm, 1.5−3 mJ/pulse, line width ∼0.3 cm^{-1}). The absolute photolysis laser wavelength was monitored by a wavemeter (Burleigh WA-4500). The polarization of the photolysis radiation was rotated by a Fresnel-Rhomb achromatic $\lambda/2$ plate for product angular distribution measurements. The H atoms produced from the C_3H_3 photodissociation were tagged by two-color resonant excitation (121.53 nm + 366.36 nm), i.e., from 1^2S to 2^2P via the H-atom Lyman-α transition and then further to a high-*n* Rydberg state. A small fraction of the radiatively metastable Rydberg H atoms drifted with their nascent velocities toward a microchannel plate (MCP) detector that is positioned perpendicular to the molecular beam, and were field-ionized in front of the detector and detected. The nominal flight length was 37.1 cm,[27] which was calibrated by 230−250 nm photodissociation of HBr [with the spin−orbit splitting of Br($^2P_{3/2}$) and Br ($^2P_{1/2}$)].The ion signals were amplified by a fast preamplifier, and the H-atom TOF spectra were recorded and averaged by using a multichannel scaler. The H-atom TOF spectra were accumulated with ∼10^5 laser firings. Typically four types of HRTOF spectra were taken (including the full spectrum and three background spectra), and the net HRTOF spectra from the UV photolysis of the C_3H_3 radical were obtained after proper background subtraction (see the Results section for more details).

The H-atom photofragment yield (PFY) spectra (i.e., action spectra) were measured with two methods. The first method involved integrating the net HRTOF spectra (after the background removal) as a function of photolysis wavelength. The second method was based on collecting the H-atom product REMPI signals as a function of photolysis wavelength. The H-atom REMPI experiment was conducted in the same HRTOF instrument, and the photolysis and REMPI ionization lasers were the same as in the HRTOF experiment. Upon photodissociation by the UV laser radiation in the range of 230−250 nm, the product H atoms were detected by 1 + 1′ REMPI, with one Lyman-α photon resonantly exciting the H atom from 1^2S to 2^2P and a UV photon at ∼364 nm ionizing the H atom. The photolysis and REMPI probe laser delay time was fixed at 15 ns. The H^+ ions were extracted and accelerated in the linear TOF mass spectrometer, and were detected by the MCP detector. The mass-resolved ion current signal (at *m*/*z* 1, H^+) was amplified by a preamplifier, recorded in a digital storage oscilloscope, and transferred to the computer. At each UV wavelength, typically 512 laser shots were averaged. Two types of REMPI signal were recorded: (i) with the 193-nm radiation on (for the propargyl radical production), the UV photolysis radiation on, and the REMPI probe lasers on; and (ii) background with the 193-nm radiation off, but the UV photolysis radiation and the REMPI probe lasers on. The PFY spectra were the net H-atom REMPI signals with the background (ii) removed. The photolysis laser power was normalized for the H-atom PFY spectra.

REMPI spectra of the propargyl radical were also searched by using a (1 + 1) scheme. The UV laser radiation in the region of 220−280 nm was focused with a f.l. ≈ 20 cm lens onto the propargyl radicals beam, and the *m*/*z* 39 peak was directly monitored by using TOFMS.

Results

The TOF spectra of the H-atom product in the UV photodissociation of C_3H_3 were recorded in the photolysis wavelength region of 230−248 nm, with the photolysis laser polarization parallel and perpendicular to the flight path, respectively. To identify the origins of the H-atom signals and to establish procedures for background subtraction, four types of TOF spectra were taken: (1) full spectrum, with both the 193-nm radiation on (for C_3H_3 radical production) and the UV photolysis radiation on (for C_3H_3 radical photodissociation), plus the Rydberg atom tagging probe laser radiations (121.6 nm + 366.3 nm); (2) precursor background spectrum, with the 193-nm radiation off but the UV photolysis radiation on, plus the probe laser radiations; (3) radical production background spectrum, with the 193-nm radiation on but the UV photolysis radiation off, plus the probe laser radiations; and (4) probe laser background spectrum, with both the 193-nm radiation off and the UV photolysis radiation off, but only the probe radiations on. The background spectra 3 and 4 were observed to be

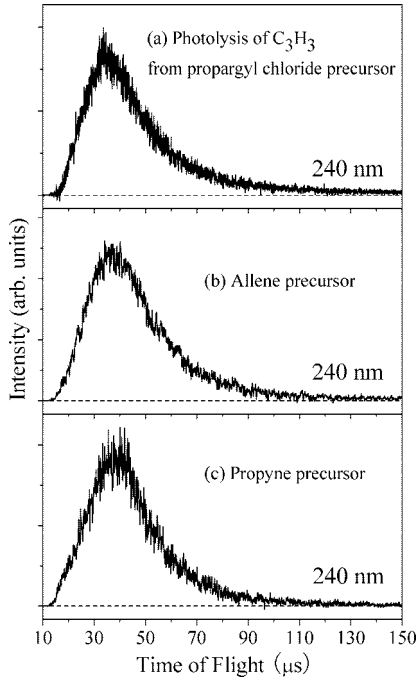

Figure 2. H-atom TOF spectra in the 240-nm photodissociation of jet-cooled C_3H_3, produced from 193-nm photolysis of (a) propargyl chloride, (b) allene, and (c) propyne. The spectra are shown as the net signals with the 193-nm photolysis laser (for radical production) on minus off. The polarization vector of the 240 photodissociation radiation is parallel ($\theta = 0°$) to the TOF axis. The photolysis radiation power intensity is 2 mJ/mm^2.

essentially identical, with only a small and broad background in the flight time range of interest, and were thus negligible. The precursor background spectrum 2 represents the main background, i.e., contributions from photolysis of the C_3H_3Cl, allene, and propyne precursors by the UV photolysis radiation. The net HRTOF spectra from the UV photolysis of the C_3H_3 radical are obtained by removing the main background 2 from the full spectrum 1. The net H-atom product TOF spectra at 240-nm photolysis wavelength with 2 mJ/mm^2 UV radiation intensity are shown in Figure 2, where panels a, b, and c represent those using propargyl chloride, allene, and propyne as the C_3H_3 radical precursor, respectively. These three TOF spectra using the C_3H_3Cl, allene, and propyne precursors are essentially the same, with a broad peak in the region of 15−120 μs and peaking around 35 μs. These common features support that the H-atom signals come from the same species, the propargyl radical. Several previous studies of the photodissociation of propargyl chloride at 193 nm reported the propargyl production, $C_3H_3Cl + h\nu \rightarrow C_3H_3 + Cl$, as the main channel.[2,11,28] The 193-nm photolysis of allene and propyne has also been studied before,[15,21,29−31] and the $H + C_3H_3$ product channel was shown to be the primary process in both allene and propyne photolysis. Indeed, 193-nm photolysis of propargyl chloride, allene, and propyne has been used previously for propargyl radical productions.[11,15]

To further confirm that the observed HRTOF spectra originate from the photolysis of propargyl radicals, two types of action or PFY spectra, integral HRTOF intensity as a function of photolysis wavelength and H-atom PFY spectrum using H-atom (1 + 1′) REMPI, were obtained. The resulting H-atom action spectra from 230 to 250 nm are scaled at 240 nm and plotted in Figure 3. The full diamonds and open diamonds represent the HRTOF action spectra with propargyl chloride and allene as the precursors, respectively. The full triangles are for the

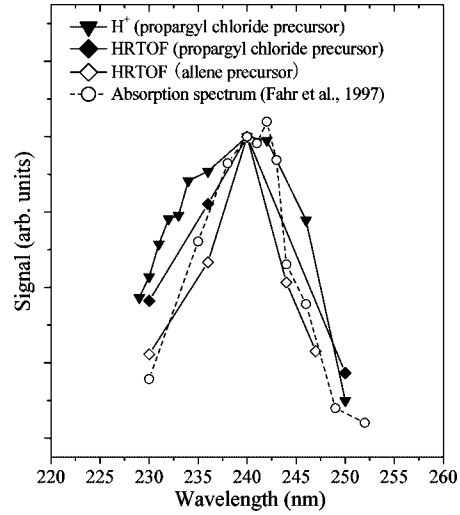

Figure 3. H-atom product yield (PFY) spectra as a function of photolysis excitation energy in the region of 229−250 nm. Diamonds represent the integrated HRTOF signals: ◆ for the C_3H_3Cl precursor and ◇ for the allene precursor. Triangles (▼) represent the H-atom (1 + 1′) REMPI signals for the C_3H_3Cl precursor. Open circles and the dashed line are the absorption spectrum taken from ref 11. The photolysis laser power is normalized for the PFY spectra. The PFY spectra and the absorption spectrum are scaled at 240 nm.

H-atom REMPI action spectrum with the propargyl chloride precursor. For comparison, the UV absorption spectrum previously reported by Fahr et al. is plotted as open circles and a dashed line in Figure 3.[11] The H-atom PFY spectra from HRTOF and REMPI agree well with each other, as well as with the UV absorption spectrum by Fahr et al. This comparison provides further confirmation that the H-atom signals originate from the photodissociation of propargyl radicals and that the strong UV absorption feature peaking at 240 nm is due to the propargyl radical. Attempts were also made to search for the REMPI spectra of propargyl by directly monitoring the *m/z* 39 peak via the (1 + 1) scheme. As the ionization potential of propargyl is 8.68 eV,[32,33] two photons at $\lambda \leq 285$ nm are sufficient to ionize the propargyl radical. However, no C_3H_3 REMPI spectrum was found near 240 nm, likely due to the fast decay of the electronically excited propargyl (in a time scale of 50 ± 10 fs)[34] and the dissociation of the propargyl radical. In addition, both H-atom PFY spectra and *m/z* 39 C_3H_3 REMPI spectra were searched for the theoretically predicted dipole-allowed $3^2B_1 \leftarrow \tilde{X}^2B_1$ transition near 220 nm and dipole-forbidden $2^2B_2 \leftarrow \tilde{X}^2B_1$ transition near 260 nm,[10,17] but no C_3H_3 absorption features were identified in these two regions, in disagreement with the theory.

The net H-atom TOF spectra of the jet-cooled C_3H_3 photodissociation are transformed to the total center-of-mass (CM) translational energy distributions, $P(E_T)$′s. The CM translational energy of product, E_T, is converted from the H-atom flight time t_H by using the following equation:

$$E_T = \left(1 + \frac{m_H}{m_{C_3H_2}}\right)E_H + \frac{m_H}{m_{C_3H_2}}E_{C_3H_3} = \frac{1}{2}m_H\left(1 + \frac{m_H}{m_{C_3H_2}}\right)\left(\frac{L}{t_H}\right)^2 + \frac{m_H}{m_{C_3H_2}}E_{C_3H_3}$$

where E_H and $E_{C_3H_3}$ are the laboratory translational energies of the H-atom photofragment and the C_3H_3 radical, respectively, and L is the flight length. The second term $(m_H/m_{C_3H_2})E_{C_3H_3}$ is

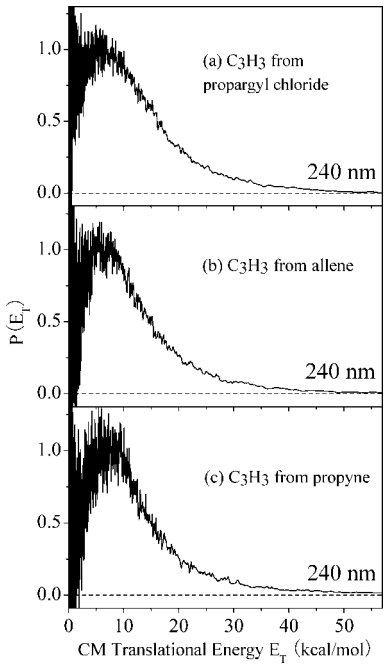

Figure 4. Center-of-mass product translational energy distributions, $P(E_T)$, of the $H + C_3H_2$ product channel from 240-nm photodissociation of C_3H_3. These distributions are converted from the H-atom TOF spectra shown in Figure 2. Panels a, b, and c correspond to the propargyl chloride, allene, and propyne precursor, respectively, for producing the C_3H_3 radicals.

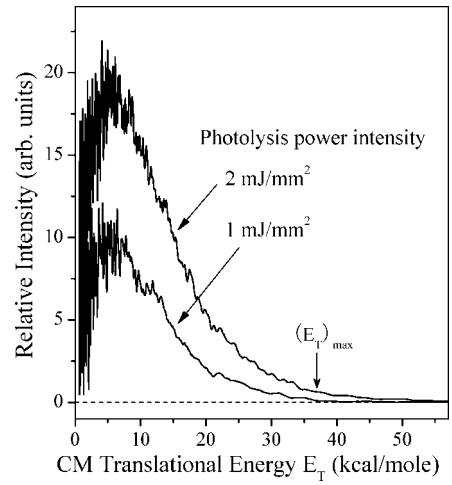

Figure 5. Photolysis laser power dependence at 2 and 1 mJ/mm^2. The spectra are directly converted from the H-atom TOF and are normalized to the same number of laser shots. Propargyl chloride precursor was used. The vertical arrow indicates the maximum translational energy release for a one-photon photodissociation of C_3H_3 at 240 nm.

due to the C_3H_3 radical motion in the molecular beam that is orthogonal to the TOF path, but it is negligible compared with the first term (products' CM translation). In this experiment, the correction due to $(m_H/m_{C_3H_2})E_{C_3H_3}$ is ~0.04 kcal/mol, based on an estimated beam velocity of 560 m/s for the C_3H_3/Ar gas mixture. The resulting $P(E_T)$ distributions of the 240-nm photodissociation of C_3H_3 with use of (a) proparpyl chloride, (b) allene, and (c) propyne precursors are shown in Figure 4. These $P(E_T)$'s are relative probability distributions (scaled to the peak height). These CM translation energy distributions for the $H + C_3H_2$ products from the three different precursors of C_3H_3 agree well with each other. The $P(E_T)$ distributions have a broad feature that peaks at low energy around 5 kcal/mol and extends to a large translational energy of ~55 kcal/mol. The bond dissociation energy (BDE) for the lowest energy H-atom loss channel, c-$C_3H_2 + H$, is calculated to be 82.4 kcal/mol in high-level theory,[19] while the heat of reaction for this dissociation channel is estimated to be 86.2 kcal/mol at 0 K and 85.6 kcal/mol at 298 K, based on thermochemistry and theoretical calculations.[19,20,24] Our preliminary study on the near-UV photolysis of C_3H_3 in the region of 278−357 nm and its H-atom PFY spectrum[35] indicate that the H-atom loss threshold is around 82.8 ± 0.3 kcal/mol, in good agreement with the 82.4 kcal/mol BDE. On the basis of this theoretical BDE value of 82.4 kcal/mol, the maximum translational energy release of the H loss channel in one-photon photodissociation of propargyl at 240 nm is 36.7 kcal/mol.

Figure 5 shows the translational energy distribution and the power dependence at 240 nm with the propargyl chloride precursor. The $P(E_T)$ distributions here are converted directly from the H-atom TOF spectra, without being normalized to the integrated area or peak height. The main peak at ~5 kcal/mol in the $P(E_T)$ distribution has a linear dependence on the photolysis laser power, in agreement with a one-photon photodissociation process, $C_3H_3 + h\nu \rightarrow H + C_3H_2$. However, in the high translational energy region (from ~37 to 55 kcal/mol), it increases nonlinearly with the increase of the photolysis power intensity (from 1 to 2 mJ/mm^2), which indicates that these fast H-atom signals, although relatively small, come from multiphoton photodissociation of C_3H_3. Indeed, the maximum translational energy release in the $P(E_T)$ distribution at the lower photolysis power intensity of 1 mJ/mm^2 is close to 36.7 kcal/mol, consistent with the expected upper limit in a one-photon process and the C−H bond dissociation energy of C_3H_3. While the $P(E_T)$ distributions presented here are obtained by direct conversion of the TOF spectra, they can also be derived from modeling the TOF spectra in a forward-convolution procedure.[36,37] In this procedure, the H-atom TOF spectrum is calculated by using a trial CM translational energy distribution $P(E_T)$ convoluted with the instrument and molecular beam functions. The calculated TOF spectrum is iteratively optimized by comparison with the experimental spectrum and readjustment of the trial $P(E_T)$ distribution until an optimized $P(E_T)$ distribution is reached. The forward-convolution approach is particularly helpful when the TOF spectra are noisy, such as those at low photolysis power. Figure 6 shows the fitted TOF spectrum of the 240-nm photodissociation of C_3H_3 at low photolysis energy intensity 1 mJ/mm^2 (from Figure 5) and the optimized $P(E_T)$ distribution.

The $P(E_T)$ distributions from the direct conversion are used to calculate the average translation energy releases, $\langle E_T \rangle$, up to the one-photon maximum E_T. For example, $\langle E_T \rangle$ at 240 nm is 11.1, 11.2, and 11.5 kcal/mol for the propargyl chloride, allene, and propyne precursor, respectively. The $\langle E_T \rangle$ values averaged from the three precursors are listed as a function of photolysis wavelength in Table 1. These $\langle E_T \rangle$ values are the upper limits due to the small contributions from the multiphoton processes. Alternatively, $\langle E_T \rangle$ can be calculated from the $P(E_T)$ distributions derived from the forward-convolution of TOF spectra at low photolysis power. For example, $\langle E_T \rangle$ at 240 nm is calculated to be 10.0 kcal/mol for the 1 mJ/mm^2 photolysis power (Figures 5 and 6), and this $\langle E_T \rangle$ value is at the lower limit. The $\langle E_T \rangle$ values in Table 1 could be overestimated by up to ~10%. As shown in Table 1, $\langle E_T \rangle$ increases with the increasing photolysis photon energy and excess energy, while the fraction of $\langle E_T \rangle$ in the total available energy, $\langle f_T \rangle$, increases only slightly between 0.29 and 0.33 and is close to a constant. The $P(E_T)$ peak position

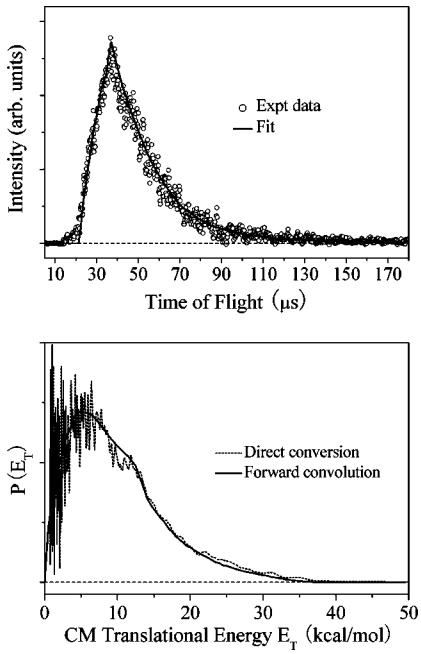

Figure 6. The 240-nm photodissociation of C_3H_3 (from propargyl chloride precursor) at low photolysis laser power 1 mJ/mm^2: (a) forward-convolution fitting of the TOF spectrum and (b) CM translational energy distribution optimized in the forward-convolution procedure compared with that derived from direct conversion. See text for more details.

TABLE 1: Photolysis Wavelength, Translational Energy Release (in kcal/mol), and Anisotropy Parameter β in the UV Photodissociation of the Propargyl Radical

photolysis wavelength (nm)	$(E_T)_{max}$[a]	$\langle E_T \rangle$[b]	$\langle f_T \rangle$[c]	β
230	41.8	13.8	0.33	0.0
236	38.7	12.5	0.32	0.0
240	36.6	11.3	0.31	0.0
244	34.7	10.4	0.30	0.0
248	32.8	9.5	0.29	0.0

[a] Maximum translational energy release, derived from the corresponding photon energy and the dissociation of propargyl to the H + *c*-C_3H_2 products, $D_0(H-C_3H_2)$ = 82.4 kcal/mol. The $D_0(H-C_3H_2)$ is in the range of 82.4−86.2 kcal/mol, estimated from both theories and thermochemistry data.[19,20,24] [b] Average translational energy release calculated from the experimental $P(E_T)$ distributions and averaged over the three precursors (whenever available). [c] Fraction of average translational energy release in the total available energy.

is at ∼5 kcal/mol and does not change significantly with the photolysis wavelength. For all the wavelengths, the $P(E_T)$ peak position is smaller than the average translational energy release.

The H-atom product angular distributions in the UV photodissociation of propargyl are examined by using linearly polarized laser radiation. Figure 7 (upper two panels) illustrates the H-atom TOF spectra from the C_3H_3 photodissociation by the polarized 240-nm photolysis radiation, with the polarization direction parallel and perpendicular to the TOF axis. The two TOF spectra are identical, indicating an isotropic H atom product angular distribution. The linearly polarized light preferentially excites those radicals with their electronic transition dipole moment parallel to the electric ***E*** of the polarized laser radiation. The photofragment angular distribution is given by $I(\theta) = (1/4\pi)[1 + \beta P_2(\cos\theta)]$, where β is the anisotropy parameter ($-1 \le \beta \le 2$), θ is the angle between the electric vector of the polarized laser radiation ***E*** and the recoiling velocity vector of

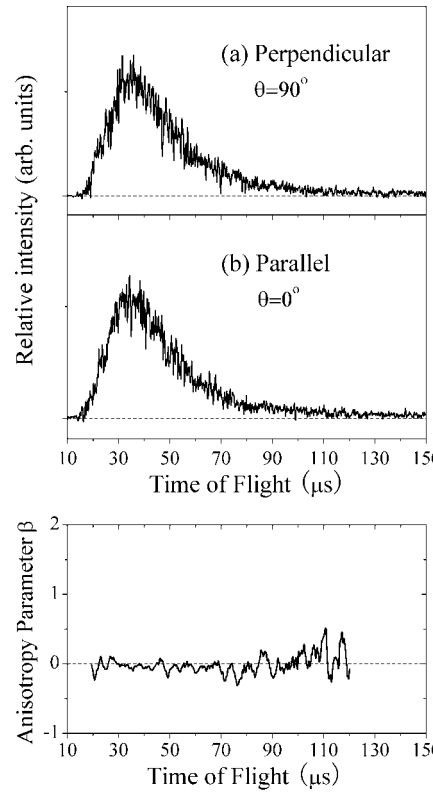

Figure 7. H-atom TOF spectra of 240-nm photodissociation of C_3H_3, with the polarization **E** vector of the photolysis radiation (a) perpendicular ($\theta = 90°$) and (b) parallel ($\theta = 0°$) to the TOF axis. The 240-nm radiation power intensity was 2 mJ/mm^2. The signals have been normalized to the same photolysis power and laser shots. Anisotropy parameter β is plotted as a function of H-atom time-of-flight. The β parameter stays very close to the limit of an isotropic angular distribution.

the H-atom product (the direction of detection or the TOF axis), and $P_2(\cos\theta)$ is the second Legendre polynomial.[38] By using this equation and the H-atom TOF spectra at 240 nm, an anisotropy parameter $\beta \approx 0$ is derived for the H + C_3H_2 product channel in the C_3H_3 photodissociation (Figure 7). For other photolysis wavelengths in this UV region, the β parameters of the summed H-atom signals in the H-atom TOF spectra are calculated and listed in Table 1; these β parameters are essentially the same within experimental error and are at the limit of $\beta = 0$ for isotropic angular distribution. The isotropic product angular distributions are consistent with a dissociation time scale of more than one rotational period of the C_3H_3 radical (> ps).[38]

The H-atom yield time profile in the UV photolysis of propargyl is also monitored as a function of the photolysis laser and probe laser delay time (Figure 8), which provides a measurement for the microcanonical rate of unimolecular dissociation of propargyl. In this time profile, the initial rise indicates the rate for H-atom production from the propargyl radical, while the decay of signal after the peak is simply due to flight out of the H atoms from the interaction region between the photolysis and probe laser pulses.[12] The H-atom signal monotonically decays after the initial rise within the 10 ns overlapping window of the photolysis and probe lasers (i.e., the time resolution of the 7 ns pump and probe pulses in this experiment). As a calibration system, UV photolysis of the SH radical, which has a fast dissociation time of *sub*-picoseconds in a direct repulsive dissociation,[27] was checked, and the delay time profile of its H-atom product was recorded. The H-atom

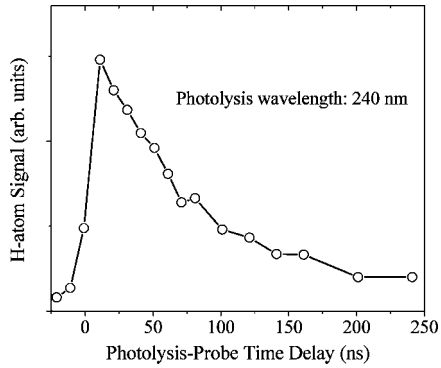

Figure 8. H-atom product signal as a function of photolysis and probe laser delay time. Propargyl chloride is the precursor. The photolysis wavelength is 240 nm. The signals are obtained by H-atom product REMPI spectra at various photolysis-probe delay times.

time profile from propargyl is very similar to that of the SH radical. This indicates that the H-atom products from propargyl rise to the maximum within the 10 ns time resolution of this experiment, and the dissociation time scale of propargyl at 240 nm is <10 ns or the dissociation rate is $>10^8$ s^{-1}. The dissociation time of propargyl observed in this study is much shorter than the ~100 ns appearance time of H atoms (i.e., dissociation rate of 1.3×10^7 s^{-1} at 242 nm) by Chen and co-workers.[12]

Discussion

The main motivations for this study are to probe the UV photodissociation dynamics of C_3H_3, confirm the previously observed broad absorption peak and the H-atom photodissociation signals of C_3H_3 near 240 nm,[11,12] and examine the theoretical predications of the electronic excited states and UV absorption spectrum of C_3H_3 by Eisfeld.[10] The broad UV absorption band of propargyl at 242 nm was first reported by Fahr et al. using the C_3H_3Cl and C_3H_3Br precursors,[11] and it was then supported by the H-atom PFY spectrum in the UV photodissociation of propargyl using the C_3H_3Br precursor,[12] the more recent absorption study by Fahr et al. using the allene, propyne and 2-butyne precursors,[15] and the most recent 248-nm photodissociation study of C_3H_3 using the allene precursor.[23] This strong broad UV absorption band, however, was questioned previously by absorption experiments,[9,13,14] which attributed it to the chlorine and bromine adducts of propargyl halides. Furthermore, this strong UV absorption band was not confirmed by the high-level multireference configuration interaction (MRCI) calculations by Eisfeld,[10,17] which showed that for propargyl radical in the region between 180 and 280 nm both the dipole-allowed $3^2B_1 \leftarrow \tilde{X}^2B_1$ transition and dipole-forbidden $2^2B_2 \leftarrow \tilde{X}^2B_1$ transition were weak bands with vibronic structures, peaking near 220 and 260 nm, respectively.[10] Instead, the strong broad absorption feature at 242 nm was suggested to be due to vinylidene carbene (H_2CCC) or chlorine adduct of propargyl chloride.[10] The conclusion from the theory[10] questioned the validity of the H-atom photodissociation signals in the study by Chen's group.[10,12] Our current experiment, nevertheless, indicates that the propargyl radical is responsible for the observed strong broad absorption peak near 242 nm.[11] Our H-atom PFY spectra derived from both H-atom TOF spectra and REMPI mass spectra using the three different precursors, propargyl chloride, allene, and propyne, are in very good agreement with the absorption spectrum by Fahr et al. (Figure 3) and with the H-atom action spectrum by Chen's group,[12] supporting that they originate from the propargyl absorption and photodissociation. The H-atom TOF spectra and $P(E_T)$ distributions in Figures 2 and 4 for the photodissociation of propargyl with three different precursors are essentially the same, further supporting that they are from the propargyl radical. Meanwhile, no H-atom PFY spectra or C_3H_3 REMPI spectra are identified for the theoretically predicted $3^2B_1 \leftarrow \tilde{X}^2B_1$ transition (peaking near 220 nm) and $2^2B_2 \leftarrow \tilde{X}^2B_1$ transition (peaking near 260 nm).[10,17] Therefore, this study supports the strong broad absorption spectrum of propargyl near 242 nm by Fahr et al.[11] and the H-atom photodissociation signals of C_3H_3 near 240 nm by Deyerl et al.,[12] and disagrees with the theoretical predications of the UV absorption spectrum and the 2^2B_2 and 3^2B_1 electronic excited states of C_3H_3 by Eisfeld.[10,17]

The CM product translational energy distributions of the H + C_3H_2 channel from the three different precursors have very similar shape and peak position. All of these distributions are not repulsive and peak at a low kinetic energy of ~5 kcal/mol. In general, these distributions are similar to those obtained by the previous C_3H_3 photodissociation studies, detection of C_3H_2 in the secondary photolysis of C_3H_3 at 193 nm by Jackson et al.,[21] H-atom Doppler profile in the photodissociation at 242 nm by Chen's group,[12] and TOF measurements of C_3H_2 fragment in the photodissociation at 248 nm by Neumark's group.[23] Our $P(E_T)$ distributions are consistent with a dissociation mechanism in which internal conversion of propargyl from the electronic excited state to the ground state is followed by unimolecular dissociation on the highly vibrationally excited ground state,[20] as suggested previously by the groups of Chen[12] and Neumark.[23]

The $P(E_T)$ distribution at 193 nm by Jackson et al. peaks at ~12.5 kcal/mol with $\langle f_T \rangle \approx 0.31$ (using BDE of 82.4 kcal/mol for the lowest energy c-C_3H_2 + H channel), while our $P(E_T)$ distributions near 240 nm peak at ~5 kcal/mol with comparable $\langle f_T \rangle$ in the range of 0.29−0.33. The $P(E_T)$ distribution at 193 nm was obtained from the secondary photolysis of hot propargyl radical and thus is less reliable than those from the primary photodissociation of jet-cooled propargyl radicals. On the other hand, the $P(E_T)$ distribution at 242 nm from Chen's group peaks at ~2.5 kcal/mol with $\langle f_T \rangle \approx 0.17$ (assuming BDE of 82.4 kcal/mol), and the $P(E_T)$ at 248 nm from Neumark's group peaks at 1.8 kcal/mol with $\langle f_T \rangle \approx 0.17$ (using BDE of 82.4 kcal/mol). The last two $P(E_T)$ distributions, peaking near $E_T = 0$, are close to that predicted in a prior distribution,[12] and are consistent with the mechanism of H loss with no exit channel barrier.[12,23] Our $P(E_T)$ distributions peak at a higher energy of ~5 kcal/mol with larger $\langle f_T \rangle \approx 0.3$. While our $P(E_T)$ distributions are in general consistent with a statistical dissociation mechanism of C_3H_3 in its ground state, they have a larger E_T release than expected in the prior distribution, and it is not clear the cause for the small difference between our results and those by Chen (from the Doppler profile of H atoms) and Neumark (from the TOF spectra of C_3H_2 fragments). The H-atom REMPI Doppler profile has a much lower resolution than HRTOF, and it is difficult to extract reliable $P(E_T)$ information at the center of the Doppler profile, where components of all the H-atom signals in the direction of Doppler probe are added up, and the Doppler profile could be contaminated by slow H-atom background peaking at the center of the profile. The TOF spectra of C_3H_2, due to the heavy mass of the C_3H_2 fragments and thus little recoils from the C_3H_3 parent beam, were measured at small angles from the beam, and could potentially show interference in the low E_T part by the $C_3H_2^+$ ionization fragment from the C_3H_3 radical in the beam. In the HRTOF setup, the light H atoms are detected perpendicular to the C_3H_3 beam direction. The detection efficiency for the very

slow H atoms decreases due to the reduced detector solid angle, and the slowest ones ($E_T \approx 0.4$ kcal/mol in the He beam and 0.04 kcal/mol in the Ar beam) eventually miss the detector. For an isotropic product distribution and for a pure geometrical correction, the detection efficiency can be corrected by dividing by a factor of $[1 - (v_P/v_H)^2]^{3/2}$, where v_P and v_H are the parent beam velocity and the H atom recoil velocity, respectively.[39] The correction for the Ar beam is rather small due to the smaller $v_P \approx 560$ m/s; for example, the correction for the detection efficiency is estimated to be 10% at $E_T = 0.6$ kcal/mol, 3% at 2 kcal/mol, and 1% at 5 kcal/mol. Most of the $P(E_T)$ distributions in this study were obtained by using the Ar beam, and the observed ~5 kcal/mol peak in the $P(E_T)$ distributions is reliable and is not caused by a shift due to the detection efficiency. Furthermore, the $P(E_T)$ distributions from 240-nm photodissociation of allene in He and Ar carrier gas are compared in this study and are shown to be nearly identical (within the noise, particularly at low E_T), also supporting our $P(E_T)$ distributions. Therefore, it is concluded that the ~5 kcal/mol peak and higher $\langle f_T \rangle$ observed in our experiments are not significantly affected by the detection efficiency of slow H atoms and are thus reliable.

The average translational energy release, $\langle E_T \rangle$, in the photodissociation of propargyl increases with the increasing photon energy and excess energy (Table 1), while $\langle f_T \rangle$ increases slightly from 0.29 to 0.33. The fact that $\langle f_T \rangle$ stays nearly constant when the excess energy increases from 33 to 42 kcal/mol is largely consistent with the statistical unimolecular dissociation. As the total excitation energy increases from 115 to 124 kcal/mol, the overall dissociation rate of propargyl in its unimolecular decomposition on the ground electronic state increases (from $\sim 1.7 \times 10^{10}$ s^{-1} for the fastest dissociation channel, HCCCH(^{3}B) + H, at 240 nm, estimated by the RRKM calculations),[20] and thus the lifetime of the highly vibrationally excited C_3H_3 in its ground electronic state is shortened. The small increase of $\langle f_T \rangle$ could also indicate that energy randomization is less complete and the energy redistribution toward each degree of freedom of the H + C_3H_2 products becomes less statistical, when the lifetime of the vibrationally excited ground electronic state C_3H_3 after internal conversion becomes shorter.

The $P(E_T)$ distributions do not allow us to differentiate the three possible H + C_3H_2 product channels, c-C_3H_2(^{1}A$_1$) + H, HCCCH(^{3}B) + H, and H_2CCC(^{1}A$_1$) + H, as discussed in the previous study by Neumark's group.[23] The propargyl BDE of 82.4 kcal/mol is for the lowest energy channel, c-C_3H_2 + H. As shown in Figures 4−6, the $P(E_T)$ distributions extend to the maximum possible E_T for the c-C_3H_2 + H channel in a one-photon dissociation process of propargyl, while the next higher energy channel (also the dominant channel predicted by the RRKM calculations),[20] HCCCH(^{3}B) + H, should appear at 12.5 kcal/mol lower than the maximum E_T. The $P(E_T)$ distributions clearly show the c-C_3H_2 + H dissociation channel, while the two other H-loss channels, HCCCH(^{3}B) + H and H_2CCC(^{1}A$_1$) + H, could also contribute in the photodissociation process. As shown in the potential energy surface in Figure 1, both the HCCCH(^{3}B) + H and H_2CCC(^{1}A$_1$) + H channels are simple C−H bond rapture via loose transition states with no exit channel barriers,[18,19] while the c-C_3H_2(^{1}A$_1$) + H channel also proceeds via a barrierless H-atom loss from the c-C_3H_3 intermediate after isomerization of propargyl over a 66.4 kcal/mol barrier or a higher barrier of 86.8 kcal/mol.[19] The later pathway has an overall barrier of 4.4 kcal/mol relative to the c-C_3H_2(^{1}A$_1$) + H dissociation products.[19] However, the ~5 kcal/mol peak and $\langle f_T \rangle$ in our $P(E_T)$ distributions that are higher than those in the studies by the groups of Chen and Neumark,[12,23] as well as that in the prior distribution,[12,23] could not be explained by this barrier, as the lower isomerization pathway via the lower barrier of 66.4 kcal/mol dominates the isomerization of propargyl to the c-C_3H_3 intermediate,[20] and furthermore the final step to the c-C_3H_2 + H dissociation via the c-C_3H_3 intermediate is through a loose transition state without exit channel barrier.

The angular distributions of the H-atom product from the UV photodissociation of propargyl are shown to be isotropic (Figure 7), with the anisotropy parameter $\beta \approx 0$ from 230 to 248 nm (Table 1). This isotropic angular distribution indicates that the UV photodissociation of propargyl occurs at a time scale longer than the rotational period of the C_3H_3 radical (> ps). This isotropic distribution and the dissociation time scale are also consistent with the dissociation mechanism, which is internal conversion to the vibrationally hot ground electronic state, followed by the dissociation on the ground electronic state. In this time scale, isomerization of propargyl to the c-C_3H_3 intermediate could readily occur before its dissociation to H + c-C_3H_2.[20] In the H-atom yield time profile (Figure 8), our data indicate that at the UV photoexcitation energy of 119.0 kcal/mol (240 nm), the H-loss dissociation time of propargyl is <10 ns, and the microcanonical rate of unimolecular dissociation is $>10^8$ s^{-1}. This dissociation rate is much faster than that of 1.3×10^7 s^{-1} at 242 nm observed by Chen and co-workers.[12] The lower rate of $\sim 10^6 - 10^7$ s^{-1} (to the H + c-C_3H_2 products) was modeled by using the RRKM calculations, assuming that the vibrational frequencies of propargyl were scaled by a factor of 0.71 to account for the effects of anharmonicity and that the dissociation energy to H + c-C_3H_2 was 90 kcal/mol.[12] However, the RRKM rate calculations on a high-level potential energy surface by Nguyen et al., using their calculated vibrational frequencies of the propargyl system and BDE of 82.4 kcal/mol for c-C_3H_2 + H, predicted an overall dissociation rate of $\sim 1 \times 10^9$ s^{-1} to c-C_3H_2 + H;[20] and the rate to HCCCH(^{3}B) + H and H_2CCC(^{1}A$_1$) + H was calculated to be 1.7×10^{10} and $\sim 3 \times 10^8$ s^{-1}, respectively. These rates are much higher than those given in the previous study by Chen and co-workers.[12] The range of the dissociation time scale of propargyl in our study, from a few picoseconds to less than 10 ns, is more consistent with the RRKM rates calculated by Nguyen et al.[20]

Conclusion

The H-atom product channel in the UV photodissociation of jet-cooled propargyl is studied in the wavelength region of 230 to 250 nm by using HRTOF and REMPI techniques. The PFY spectra of the H + C_3H_2 product channel obtained with propargyl chloride, allene, and propyne precursors have a broad peak near 240 nm and are in good agreement with the UV absorption spectrum of C_3H_3. The H + C_3H_2 product translational energy distribution peaks at ~5 kcal/mol, with $\langle f_T \rangle \approx 0.3$. The H-atom product has an isotropic angular distribution. The dynamic information indicates that the UV photodissociation mechanism of propargyl is internal conversion of the electronically excited propargyl followed by unimolecular decomposition on the ground state. While our H-atom PFY spectra support the previously observed UV absorption spectrum near 240 nm by Fahr et al. and our $P(E_T)$ distributions are in general agreement with those from the UV photodissociation of propargyl by Chen and co-workers and Neumark and co-workers, no H-atom action spectrum or C_3H_3 REMPI spectrum are observed for the predicted UV absorption bands in the recent theoretical calculations by Eisfeld.

Acknowledgment. This work is supported by the National Science Foundation (CHE-0416244).

Note Added after ASAP Publication. This article posted ASAP on March 10, 2009. The caption to Figure 1 and paragraph 6, sentence 4 of the Introduction have been revised. The correct version posted on March 12, 2009.

References and Notes

(1) Kern, R. D.; Chen, H.; Kiefer, J. H.; Mudipalli, P. S. *Combust. Flame* **1995**, *100*, 177.
(2) Morter, C. L.; Farhat, S. K.; Adamson, J. D.; Glass, G. P.; Curl, R. F. *J. Phys. Chem.* **1994**, *98*, 7029.
(3) Miller, J. A.; Klippenstein, S. J. *J. Phys. Chem. A* **2003**, *107*, 7783.
(4) Richter, H.; Howard, J. B. *Prog. Energy Combust. Sci.* **2000**, *26*, 565.
(5) Farmer, J. B.; Lossing, F. P. *Can. J. Chem.* **1955**, *33*, 861.
(6) Ramsay, D. A.; Thistlethwaite, P. *Can. J. Phys.* **1966**, *44*, 1381.
(7) Jacox, M. E.; Milligan, D. E. *Chem. Phys.* **1974**, *4*, 45.
(8) Wyss, M.; Riaplov, E.; Maier, J. P. *J. Chem. Phys.* **2001**, *114*, 10355.
(9) Atkinson, D. B.; Hudgens, J. W. *J. Phys. Chem. A* **1999**, *103*, 4242.
(10) Eisfeld, W. *J. Phys. Chem. A* **2006**, *110*, 3903.
(11) Fahr, A.; Hassanzadeh, P.; Laszlo, B.; Huie, R. E. *Chem. Phys.* **1997**, *215*, 59.
(12) Deyerl, H.-J.; Fischer, I.; Chen, P. *J. Chem. Phys.* **1999**, *111*, 3441.
(13) Giri, B. R.; Hippler, H.; Olzmann, M.; Unterreiner, A. N. *Phys. Chem. Chem. Phys.* **2003**, *5*, 4641.
(14) Atkinson, D. B.; Hudgens, J. W. *J. Phys. Chem. A* **1999**, *103*, 7978.
(15) Fahr, A.; Laufer, A. H. *J. Phys. Chem. A* **2005**, *109*, 2534.
(16) Honjou, H.; Yoshimine, M.; Pacansky, J. *J. Phys. Chem.* **1987**, *91*, 4455.
(17) Eisfeld, W. *Phys. Chem. Chem. Phys.* **2005**, *7*, 3924.
(18) Vereecken, L.; Pierloot, K.; Peeters, J. *J. Chem. Phys.* **1998**, *108*, 1068.
(19) Nguyen, T. L.; Mebel, A. M.; Kaiser, R. I. *J. Phys. Chem. A* **2001**, *105*, 3284.
(20) Nguyen, T. L.; Mebel, A. M.; Lin, S. H.; Kaiser, R. I. *J. Phys. Chem. A* **2001**, *105*, 11549.
(21) Jackson, W. M.; Anex, D. S.; Continetti, R. E.; Balko, B. A.; Lee, Y. T. *J. Chem. Phys.* **1991**, *95*, 7327.
(22) McCunn, L. R.; FitzPatrick, B. L.; Krisch, M. J.; Butler, L. J.; Liang, C.-W.; Lin, J. J. *J. Chem. Phys.* **2006**, *125*, 133306/1.
(23) Goncher, S. J.; Moore, D. T.; Sveum, N. E.; Neumark, D. M. *J. Chem. Phys.* **2008**, *128*, 114303.
(24) Wheeler, S. E.; Robertson, K. A.; Allen, W. D.; Schaefer, H. F.; Bomble, Y. J.; Stanton, J. F. *J. Phys. Chem. A* **2007**, *111*, 3819.
(25) Xu, K. S.; Amaral, G.; Zhang, J. S. *J. Chem. Phys.* **1999**, *111*, 6271.
(26) Amaral, G.; Xu, K. S.; Zhang, J. S. *J. Chem. Phys.* **2001**, *114*, 5164.
(27) Zhou, W.; Yuan, Y.; Chen, S.; Zhang, J. *J. Chem. Phys.* **2005**, *123*, 054330/1.
(28) McCunn, L. R.; Bennett, D. I. G.; Butler, L. J.; Fan, H.; Aguirre, F.; Pratt, S. T. *J. Phys. Chem. A* **2006**, *110*, 843.
(29) Sun, W.; Yokoyama, K.; Robinson, J. C.; Suits, A. G.; Neumark, D. M. *J. Chem. Phys.* **1999**, *110*, 4363.
(30) Ni, C.-K.; Huang, J. D.; Chen, Y. T.; Kung, A. H.; Jackson, W. M. *J. Chem. Phys.* **1999**, *110*, 3320.
(31) Qadiri, R. H.; Feltham, E. J.; Hendrik Nahler, N.; Perez Garcia, R.; Ashfold, M. N. R. *J. Chem. Phys.* **2003**, *119*, 12842.
(32) Lossing, F. P. *Can. J. Chem.* **1972**, *50*, 3973.
(33) Gilbert, T.; Pfab, R.; Fischer, I.; Chen, P. *J. Chem. Phys.* **2000**, *112*, 2575.
(34) Zierhut, M.; Noller, B.; Schultz, T.; Fischer, I. *J. Chem. Phys.* **2005**, *122*, 094302.
(35) Zheng, X. F.; Song, Y.; Wu, J.; Zhang, J. S. Unpublished.
(36) Zhao, X. Ph.D. Thesis, University of California, Berkeley, 1988.
(37) Myers, J. D. Ph.D. Thesis, University of California, Berkeley, 1993.
(38) Zare, R. N. *Photochemistry* **1972**, *4*, 1.
(39) Qadiri, R. H.; Feltham, E. J.; Cottrill, E. E. H.; Taniguchi, N.; Ashfold, M. N. R. *J. Chem. Phys.* **2002**, *116*, 906.

JP8113336